

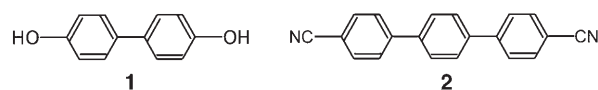
## Surface-Assisted Assembly of 2D Metal–Organic Networks That Exhibit Unusual Threefold Coordination Symmetry\*\*

Sebastian Stepanow, Nian Lin,\* Dietmar Payer, Uta Schlickum, Florian Klappenberger, Giorgio Zoppellaro, Mario Ruben, Harald Brune, Johannes V. Barth, and Klaus Kern

Coordination-based supramolecular chemistry,<sup>[1]</sup> with its characteristic control of the self-assembly process and intrinsic defect tolerance, has been proven to be a very efficient synthetic tool to fabricate metallosupramolecular networks of well-defined topology in one, two, and three dimensions.<sup>[2–8]</sup> This strategy was recently applied to low dimensions by assembling regular molecular architectures from organic molecules and transition-metal centers directly on solid surfaces.<sup>[9,10]</sup> A variety of surface-supported molecular network structures has been made accessible by the general application of a surface-assisted metal-coordination method to metal centers and aromatic polycarboxylic acids on metal surfaces.<sup>[9]</sup> As valid for supramolecular structures in general, the structures of the two-dimensional metal–organic coordination networks (2D-MOCNs) formed are predetermined by the properties of the ligands (e.g., donor atoms and their spatial arrangement, steric crowding) and the electronic characteristics of the metal ions (e.g., involved orbitals, ionization energies). However, under 2D conditions, the realization of a given coordination algorithm might be altered by the presence of a metal substrate, which results in deviating coordination geometries for the same metal–ligand coupling in comparison to the 3D situation (e.g., in the bulk phase). Such deviation can be attributed to charge transfer or screening effects and the strict 2D confinement of ligands and metal centers imposed by the substrate, which substantially influences the characteristics of the metal-to-ligand bonding within the 2D coordination network.<sup>[10e]</sup>

A study of surface-assisted coordination of iron and cobalt centers with polycarboxylic acids has revealed orthogonally arranged 2D-MOCNs exhibiting even, mostly fourfold, symmetry. In contrast, 2D-MOCNs exhibiting threefold symmetry, such as honeycomb structures or similar ones with more complexity, such as kagomé lattices, have not yet been observed on surfaces. Also in the 3D bulk phase, metal–organic coordination network structures that exhibit an odd-numbered symmetry are much less frequently observed than their even-symmetry counterparts.<sup>[11]</sup> However, a series of 2D hexagonal supramolecular structures was constructed through multiple hydrogen-bonding interactions on different surfaces by using specifically designed organic molecules.<sup>[12]</sup>

Herein we report two surface-supported 2D-MOCNs that exhibit threefold symmetry. Extended hexagonal coordination networks are formed either from iron centers with linear 4,4'-biphenol ligands (**1**) or from cobalt centers with linear 1,4';4',1''-terphenyl-4,4''-dicarbonitrile ligands (**2**) on copper or silver single-crystal surfaces. We have shown by using



substrates with different symmetries that the threefold symmetry is intrinsic to the metal–ligand coordination and is not due to geometrical templating effects of the underlying surfaces.

STM topographs of the coordination node of the network formed by Fe centers and three ligands **1** on an Ag(111) surface and a Cu(100) surface are shown in Figure 1a and Figure 1b, respectively. Both reveal a local threefold symmetry, which implies one iron center and three ligands. A model is shown in Figure 1c, in which we assume that under the experimental conditions the molecules of ligand **1** are adsorbed with the aromatic rings parallel to the surface plane and that there is no distortion of molecules in comparison with those of the gas phase. Furthermore, X-ray photoemission-spectroscopy measurements reveal that the phenol groups are deprotonated resulting in negatively charged phenolates.<sup>[13]</sup> The deprotonation process is induced by the catalytic activity of the metallic surfaces and the deposited Fe, which was also observed in studies with more-acidic aromatic polycarboxylic acids.<sup>[14–16]</sup> The Fe–O bond lengths amount to  $(2.0 \pm 0.3)$  Å and the estimated O–Fe–O angles vary from 100 to 140°, depending on the overall network structures. However, with respect to the underlying substrate, the exact positions of the iron atoms and molecules

[\*] Dr. S. Stepanow, Dr. N. Lin, D. Payer, Prof. K. Kern  
Max-Planck-Institut für Festkörperforschung  
Heisenbergstrasse 1, 70569 Stuttgart (Germany)  
Fax: (+49) 711-6891662  
E-mail: n.lin@fkf.mpg.de

Dr. U. Schlickum, Dr. F. Klappenberger, Prof. H. Brune,  
Prof. J. V. Barth, Prof. K. Kern  
Institut de Physique des Nanostructures  
Ecole Polytechnique Fédérale de Lausanne  
1015 Lausanne (Switzerland)

Dr. G. Zoppellaro, Dr. M. Ruben  
Institut für Nanotechnologie, Forschungszentrum Karlsruhe  
76021 Karlsruhe (Germany)

Prof. J. V. Barth  
Departments of Chemistry and Physics & Astronomy  
The University of British Columbia  
Vancouver, BC V6T1Z4 (Canada)

[\*\*] This work was supported partially by the EC-FP VI STREP “BIOMACH” (NMP4-CT-2003-505-487) and by the ESF-EURO-CORES-SONS project “FunSMARTs”.

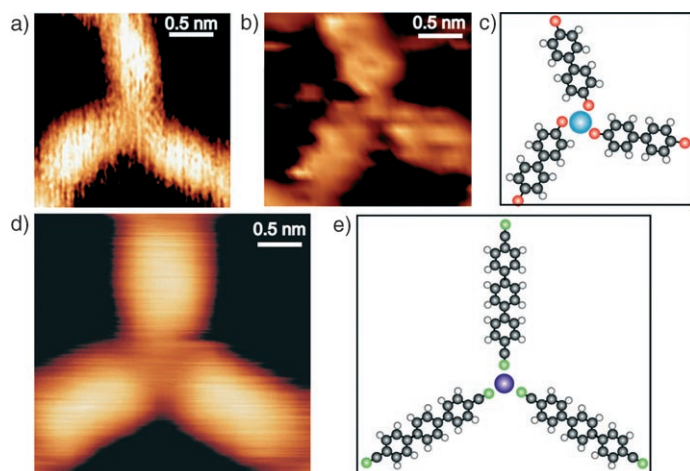


**Figure 1.** STM topographs of the threefold Fe(biphenolate)<sub>3</sub> network node on a) an Ag(111) surface, and b) a Cu(100) surface. c) Model of the threefold binding of the nodal Fe(biphenolate)<sub>3</sub> motif. d) STM topograph of the threefold Co(dicarbonyl)<sub>3</sub> network node on an Ag(111) surface. e) Model of the threefold binding of the nodal Co(dicarbonyl)<sub>3</sub> motif. For (a) and (b) the image was taken at a tunnel current of 0.1 nA and a bias voltage of 0.5 V, for (d) a tunnel current of 0.3 nA and a bias voltage of 1.9 V. C gray; H white; O red; N green; Fe light blue; Co dark blue.

1 remain unknown as simultaneous resolution of the atomic lattice of the surfaces was not achieved in our measurements. The STM data elucidate that the ligands do not point directly towards the central Fe atom but rather tilt clockwise (*R*) or anticlockwise (*S*) which accounts for the 2D chirality.<sup>[17]</sup>

A second example of threefold coordination, the coordination of cobalt with **2** on an Ag(111) surface, is shown in Figure 1 d. The STM data imply that a mononuclear Co center is coordinated by three carbonitrile groups of **2**, as shown by the model in Figure 1 e. The N-Co-N angles are close to the ideal value of 120°. In contrast to the Fe–phenolate coordination, the three linear carbonitrile ligands point symmetrically to the central Co atom. Therefore, the resulting coordination node does not exhibit any chirality.

In 3D bulk phases, the coordination of iron centers to phenolates leads exclusively to six-, five-, or fourfold coordination motifs;<sup>[18]</sup> to our knowledge, threefold coordination is not yet known. Similarly, benzonitrile and acetonitrile complexes of a multitude of d- and f-block metals are well-known and have been investigated,<sup>[19]</sup> but purely threefold coordination has not yet been observed. The emergence of unusual coordination geometries and coordination numbers in this study can be attributed to the very peculiar 2D environment of the metal surfaces not encountered in the conventional 3D coordination. The substrates cause rehybridization of the orbitals of the metal centers in the surface-supported MOCNs,<sup>[9e]</sup> which leads to unusual redox states for these metal centers. The tendency of the mostly  $\pi$  aromatic ligands to adopt a flat configuration at the surface can stabilize unusual coordination modes. Furthermore, the absence of solvent and gas molecules, which in bulk synthesis are very often able to occupy open coordination sites, may result in the

formation of coordinatively unsaturated complexes under ultrahigh vacuum (UHV) conditions.

Figure 2a displays the overall network structure of the Fe–**1** system developed on an Ag(111) surface. Two types of hexagons, which are indicated by *T* and *C* in Figure 2a, can be detected. The *T*-type hexagons have  $C_3$  symmetry, while the *C*-type hexagons are compressed in one direction. Both types of hexagon lead to a nearest-neighbor Fe–Fe separation of

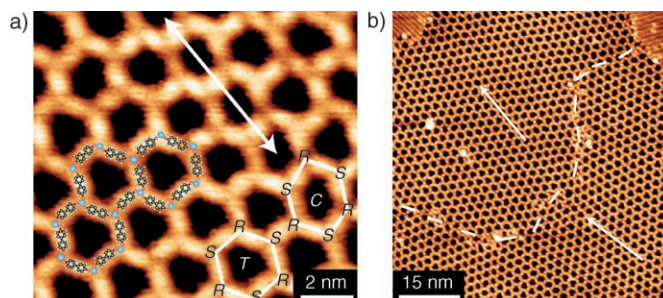
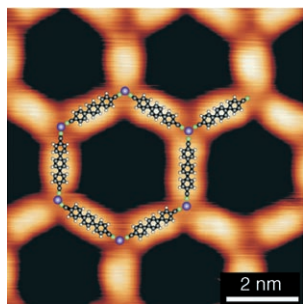


**Figure 2.** STM topographs displaying the hexagonal Fe–biphenolate network assembled on Ag(111). a) A high-resolution STM image. A tentative model is superimposed on the data with the same color code as that used in Figure 1. The *T*-type and *C*-type hexagons are highlighted in white frames. The double arrow indicates a ribbon of hexagons only consisting of *C* hexagons. *R* and *S* denote the clockwise and anticlockwise folding, respectively, of the three biphenolate ligands **1** around each iron center. b) An overview showing two domains that are separated by a domain boundary (dashed line). The white arrows mark the domain orientations. The image was taken at a tunnel current of 0.1 nA and a bias voltage of 0.5 V.

approximately 13 Å. The O–Fe–O angles of the *T* hexagons amount to 120°, as expected for a perfect honeycomb. For the *C* cavity, the O–Fe–O angles deviate by about 20° from the ideal value of 120°. Both the *T*-type and the *C*-type hexagons have alternately arranged *R* and *S* nodes (*-RSRSRS-*), as shown in Figure 2a. The overall ratio of the two enantiomeric chiral centers is balanced, thus resulting globally in a 2D racemate.

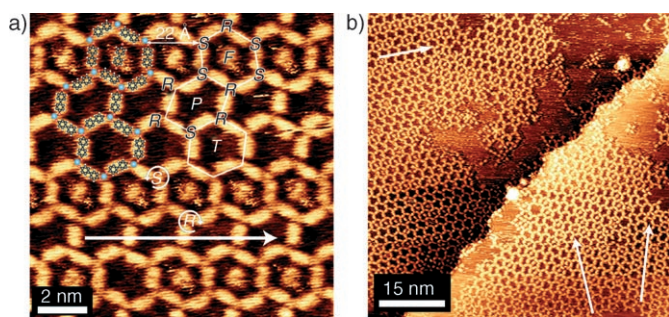
The network domains can grow continuously over the entire terraces of the Ag(111) surface and frequently exceed 100 nm. Figure 2b shows two domains with different orientations (indicated by two arrows), which enclose an angle of  $(14.5 \pm 1)^\circ$ . The domain boundary (marked by the dashed line) comprises distorted hexagons as well as pentagon–heptagon lattice faults. The *C* hexagons tend to align in straight rows that go through a single domain, as indicated by the arrow in Figure 2a. At relatively low coverage, when the surface is not yet fully occupied by the network, the *T*-type hexagons predominate. The *C*-type hexagons evolve when the network coverage is close to a full adlayer. Clearly, the lack of open space favors a compression of the network structure.

Figure 3 shows the hexagonal Co–**2** network on an Ag(111) surface. The formation of highly symmetric hexagons is predominant in this network as a consequence of the symmetric achiral coordination nodes. In each of the hexagons formed, the separation between two oppositely faced Co atoms is about 38 Å and a nearest-neighbor distance between Co atoms is about 19 Å.



**Figure 3.** A high-resolution STM image of the honeycomb network of Co-2 on Ag(111). A tentative model is superimposed onto the data with the same color code as that used in Figure 1. The image was taken at a tunnel current of 0.3 nA and a bias voltage of 1.9 V.

Possible templating effects of the substrate by assembling the same Fe-biphenolate network on a Cu(100) surface that exhibits fourfold surface symmetry is discussed below. Figure 4 reveals that hexagonal networks are formed despite



**Figure 4.** STM topographs of the hexagonal Fe-biphenolate network assembled on Cu(100). a) A high-resolution STM image of the network. The arrow marks the direction of the high-symmetry row. The white polygons highlight the hexagon frame of the *P*-type, *F*-type, and *T*-type. A tentative model is superimposed on the STM data with the same color code as that used in Figure 1. b) An overview showing three differently oriented domains (shown by the white arrows). The domain size is considerably smaller on Cu(100) than on Ag(111). The image was taken at a tunnel current of 0.1 nA and a bias voltage of 0.5 V.

the mismatch between the substrate and the network nodal symmetry. Three types of hexagons are observed: The first type, denoted as *T* type, shows  $C_3$  symmetry, while the other two types reveal a low-symmetry parallelogram-like envelope, as indicated by *F* and *P* in Figure 4a. The O-Fe-O angles deviate from the ideal of  $120^\circ$  and fall in a range between  $100^\circ$  and  $140^\circ$ . Single molecules of **1** may be trapped in cavities, primarily in the hexagons of the *F* type (74% filling rate). The three types of hexagons are present in approximately the same abundance.

Although the network extends in two dimensions, a strict periodicity of 22 Å is only obeyed in one direction (indicated by the straight arrow in Figure 4a). This direction is denoted as the high-symmetry row, which consists of a single type of hexagon. Overall we observed four different high-symmetry row orientations (three are present and marked out in the

overview STM topograph of Figure 4b), which are related to each other by rotation and mirror symmetry operations of the Cu(100) surface-symmetry point groups. The domain size of the networks is substantially smaller than for those formed at the Ag(111) surface. As shown in Figure 4b the distorted hexagons (*F* and *P* types) are formed in the presence of open surface area, in contrast to the formation of the *C*-type hexagons at the Ag(111) surface, which only form when the adlayer is close to being full. Thus, this distortion is not caused by compression but rather by substrate template effects.

Despite the identical hexagonal topology, the networks formed on the fourfold Cu(100) surface differ from those formed on the threefold Ag(111) surface in: 1) the shape and organization of the hexagons; 2) the occurrence of different rotational and mirror domains; 3) the size of the single domains. These differences can be explained by template effects of the respective substrates, which cause slight displacements of the network elements from the ideal hexagonal-network positions as a result of the preferred adsorption sites of the molecules and iron atoms at the atomic lattice of the substrate. Because the nodes of a perfect hexagonal network cannot adsorb at the same lattice sites of the fourfold Cu(100) substrate, the network is deformed and forms the *F*- and *P*-type hexagons to optimize the adsorption.

Compared with the previously reported hydrogen-bonded nanometer-scale 2D hexagonal structures,<sup>[12]</sup> the metal-coordination-based hexagonal networks presented herein have several advantages: 1) higher thermal stability arising from the relatively strong coordination bonds; 2) structural flexibility, in particular that the bonding angles may deviate from  $120^\circ$ , which enables the network formation at substrates with different symmetry; 3) specific bonding, which reduces the frequently occurring structural faults in the hydrogen-bonded systems.

In conclusion, for the first time, two 2D-MOCNs expressing hexagonal topologies according to a specific local threefold coordination mode were formed on surfaces. The symmetry of the evolving coordination networks is independent of the symmetry of the substrate, which indicates that the metal-ligand coordination predominates over the substrate influences. Current work addresses the elucidation of the coordination characteristics of the metal centers involved, which will also set the basis for the investigation of the physical properties (e.g., magnetic properties) of the networks formed.

### Experimental Section

Metal atoms (Fe, Co) and organic molecules **1** and **2** were subsequently deposited on the metal surfaces in standard UHV chambers with base pressures of less than  $2 \times 10^{-10}$  mbar. The Cu(100) and Ag(111) surfaces were prepared by repeated cycles of  $\text{Ar}^+$  ion sputtering and subsequent annealing at 800 K, by which flat terraces of up to 100 nm width separated by monatomic steps were obtained. Ligand **1** was bought (Fluka Chemie GmbH, Germany; purity > 98%) and ligand **2** was synthesized following a modified procedure of a given protocol.<sup>[20]</sup> Both compounds were deposited by organic molecular beam epitaxy (OMBE) from a Knudsen cell evaporator, held at 415 K (**1**) or 460 K (**2**) during deposition. Fe/Co atoms were evaporated by using an evaporator heated with an electron beam and

a flux in the range of a few percent of a monolayer per minute. Deposition of **1** and Fe was performed at a substrate temperature of 400 K and deposition of **2** and Co at a substrate temperature of 300 K. Coverage below full monolayer saturation was employed for the molecular precursor layers to leave space for the formation of the more-open network structures. STM experiments with constant-current mode were performed in situ after samples had been cooled to room temperature or 10 K.

Received: September 6, 2006

Published online: December 8, 2006

**Keywords:** coordination modes · ligand effects · scanning probe microscopy · supramolecular chemistry · surface chemistry

- [1] J. M. Lehn, *Supramolecular Chemistry: Concepts and Perspectives*, VCH, Weinheim, **1995**.
- [2] S. Leininger, B. Olenyuk, P. J. Stang, *Chem. Rev.* **2000**, *100*, 853–908.
- [3] B. J. Holliday, C. A. Mirkin, *Angew. Chem.* **2001**, *113*, 2076–2098; *Angew. Chem. Int. Ed.* **2001**, *40*, 2022–2043, and references therein.
- [4] M. Ruben, J. Rojo, F. J. Romero-Salguero, L. H. Uppadine, J.-M. Lehn, *Angew. Chem.* **2004**, *116*, 3728–3747; *Angew. Chem. Int. Ed.* **2004**, *43*, 3644–3662.
- [5] a) B. Moulton, M. J. Zaworotko, *Chem. Rev.* **2001**, *101*, 1629, and references therein; b) S. Kitagawa, R. Kitaura, S. Noro, *Angew. Chem.* **2004**, *116*, 2388–2430; *Angew. Chem. Int. Ed.* **2004**, *43*, 2334–2375, and references therein; c) O. M. Yaghi, M. O’Keeffe, N. W. Ockwig, H. K. Chae, M. Eddaoudi, J. Kim, *Nature* **2003**, *423*, 705, and references therein.
- [6] J. Michl, T. F. Magnera, *Proc. Natl. Acad. Sci. USA* **2002**, *99*, 4788.
- [7] A. Semenov, J. P. Spatz, M. Möller, J.-M. Lehn, B. Sell, D. Schubert, C. H. Weidl, U. S. Schubert, *Angew. Chem.* **1999**, *111*, 2701–2705; *Angew. Chem. Int. Ed.* **1999**, *38*, 2547–2550.
- [8] D. G. Kurth, N. Severin, J. P. Rabe, *Angew. Chem.* **2002**, *114*, 3833–3835; *Angew. Chem. Int. Ed.* **2002**, *41*, 3681–3683.
- [9] a) A. Dmitriev, H. Spillmann, N. Lin, J. V. Barth, K. Kern, *Angew. Chem.* **2003**, *115*, 2774–2777; *Angew. Chem. Int. Ed.* **2003**, *42*, 2670–2673; b) M. A. Lingenfelder, H. Spillmann, A. Dmitriev, S. Stepanow, N. Lin, J. V. Barth, K. Kern, *Chem. Eur. J.* **2004**, *10*, 1913–1919; c) S. Stepanow, M. A. Lingenfelder, A. Dmitriev, H. Spillmann, E. Delvigne, N. Lin, X. Deng, C. Cai, J. V. Barth, K. Kern, *Nat. Mater.* **2004**, *3*, 229–233; d) N. Lin, S. Stepanow, F. Vidal, J. V. Barth, K. Kern, *Chem. Commun.* **2005**, 1681–1683; e) A. P. Seitsonen, M. A. Lingenfelder, H. Spillmann, A. Dmitriev, S. Stepanow, N. Lin, K. Kern, J. V. Barth, *J. Am. Chem. Soc.* **2006**, *128*, 5634–5635; f) S. Clair, S. Pons, S. Fabris, S. Baroni, H. Brune, K. Kern, J. V. Barth, *J. Phys. Chem. B* **2006**, *110*, 5627–5632; g) T. Classen, G. Fratesi, G. Costantini, S. Fabris, F. L. Stadler, C. Kim, S. de Gironcoli, S. Baroni, K. Kern, *Angew. Chem.* **2005**, *117*, 6298–6301; *Angew. Chem. Int. Ed.* **2005**, *44*, 6142–6145; h) S. Stepanow, N. Lin, J. V. Barth, K. Kern, *J. Phys. Chem. B* **2006**, *110*, 23472–23477
- [10] a) M. Ruben, *Angew. Chem.* **2005**, *117*, 1620–1623; *Angew. Chem. Int. Ed.* **2005**, *44*, 1594–1596; b) N. Lin, S. Stepanow, F. Vidal, K. Kern, S. Alam, S. Strömsdorfer, S. Dremov, P. Müller, A. Landa, M. Ruben, *Dalton Trans.* **2006**, 2794–2800.
- [11] a) L. R. Macgillivray, S. Subramanian, M. J. Zaworotko, *J. Chem. Soc. Chem. Commun.* **1994**, 1325–1326; b) X. Xu, M. Nieuwenhuyzen, S. L. James, *Angew. Chem.* **2002**, *114*, 790–793; *Angew. Chem. Int. Ed.* **2002**, *41*, 764–767; c) A. B. Mallik, S. Lee, E. B. Lobkovsky, *Cryst. Growth Des.* **2005**, *5*, 609.
- [12] a) J. A. Theobald, N. S. Oxtoby, M. A. Phillips, N. R. Champness, P. H. Beton, *Nature* **2003**, *424*, 1029–1031; b) S. J. H. Griessl, M. Lackinger, F. Jamitzky, T. Markert, M. Hietschold, W. M. Heckl, *J. Phys. Chem. B* **2004**, *108*, 11556–11560; c) S. De Feyter, A. Gesquière, M. Klapper, K. Müllen, F. C. De Schryver, *Nano Lett.* **2003**, *3*, 1485–1488; d) H.-J. Yan, J. Lu, L.-J. Wan, C.-L. Bai, *J. Phys. Chem. B* **2004**, *108*, 11251–11255; e) M. Stöhr, M. Wahl, C. H. Galka, T. Riehm, T. A. Jung, L. H. Gade, *Angew. Chem.* **2005**, *117*, 7560–7564; *Angew. Chem. Int. Ed.* **2005**, *44*, 7394–7398; f) N. Lin, D. Payer, A. Dmitriev, T. Strunskus, C. Wöll, J. V. Barth, K. Kern, *Angew. Chem.* **2005**, *117*, 1512–1515; *Angew. Chem. Int. Ed.* **2005**, *44*, 1488–1491; g) M. Ruben, D. Payer, A. Landa, A. Comisso, C. Gattinoni, N. Lin, J.-P. Collins, J.-P. Sauvage, A. De Vita, K. Kern, *J. Am. Chem. Soc.* **2006**, DOI:10.1021/ja063601k.
- [13] a) X.-C. Guo, R. J. Madix, *Surf. Sci.* **1995**, *341*, L1065–L1071; b) S. Stepanow, T. Strunskus, N. Lin, C. Wöll, K. Kern, unpublished results.
- [14] S. Stepanow, T. Strunskus, M. Lingenfelder, A. Dmitriev, H. Spillmann, N. Lin, J. V. Barth, C. Wöll, K. Kern, *J. Phys. Chem. B* **2004**, *108*, 19392.
- [15] a) B. G. Frederick, M. R. Ashton, N. V. Richardson, T. S. Jones, *Surf. Sci.* **1993**, *292*, 33; b) S. Poulston, R. A. Bennett, A. H. Jones, M. Bowker, *Phys. Rev. B* **1997**, *55*, 12888; c) M. Bowker, S. Haq, R. P. Holroyd, P. M. Parlett, S. Poulston, N. Richardson, *J. Chem. Soc. Faraday Trans.* **1996**, *92*, 4683; d) A. Dmitriev, N. Lin, J. Weckesser, J. V. Barth, K. Kern, *J. Phys. Chem. B* **2002**, *106*, 6907–6912.
- [16] a) N. Lin, A. Dmitriev, J. Weckesser, J. V. Barth, K. Kern, *Angew. Chem.* **2002**, *114*, 4973–4977; *Angew. Chem. Int. Ed.* **2002**, *41*, 4779–4783; b) N. Lin, D. Payer, A. Dmitriev, T. Strunskus, C. Wöll, J. V. Barth, K. Kern, *Angew. Chem.* **2005**, *117*, 1512–1515; *Angew. Chem. Int. Ed.* **2005**, *44*, 1488–1491.
- [17] a) P. Messina, A. Dmitriev, N. Lin, H. Spillmann, M. Abel, J. V. Barth, K. Kern, *J. Am. Chem. Soc.* **2002**, *124*, 14000; b) A. Dmitriev, H. Spillmann, M. Lingenfelder, N. Lin, J. V. Barth, K. Kern, *Langmuir* **2004**, *20*, 4799.
- [18] a) M. R. A. Blomberg, P. E. M. Siegbahn, *Theor. Chem. Acc.* **1997**, *97*, 72–80; b) S. Kimura, E. Bill, E. Bothe, T. Weyhermüller, K. Wieghardt, *J. Am. Chem. Soc.* **2002**, *124*, 6025–6039; c) B. Sieklucka, R. Podgajny, P. Przychodzen, T. Korzeniak, *Coord. Chem. Rev.* **2005**, *249*, 2203–2221.
- [19] a) M. H. Garcia, P. J. Mendes, A. R. Dias, *J. Organomet. Chem.* **2005**, *690*, 4063–4071; b) L. J. Moitsheki, S. A. Bourne, L. R. Nassimbeni, *Acta Crystallogr. Sect. E* **2005**, *61*, m2580–m2581; c) A. W. Zanella, K. H. Ford, P. C. Ford, *J. Am. Chem. Soc.* **1978**, *100*, 1051–1054; d) A. E. Enriquez, B. L. Scott, M. P. Neu, *Inorg. Chem.* **2005**, *44*, 7403–7413; e) C. J. Siemer, M. J. Van Stipdonk, P. K. Kahol, D. M. Eichhorn, *Polyhedron* **2004**, *23*, 235–238; f) T. Murahashi, T. Nagai, T. Okuno, T. Matsutani, H. Kurosawa, *Chem. Commun.* **2000**, 1689–1690.
- [20] J. Colonge, *Bull. Soc. Chim. Fr.* **1967**, 4370–4374.